POZNAN UNIVERSITY OF TECHNOLOGY ACADEMIC JOURNALS
No 72 Electrical Engineering 2012

Piotr GAS*

INFLUENCE OF BLOOD FLOW ON TEMPERATURE DISTRIBUTION OF HUMAN TISSUE DURING INTERSTITIAL MICROWAVE HYPERTHERMIA

This paper describes through computer simulation the utilization of the interstitial microwave hyperthermia in the treatment of pathological tissues. Electromagnetic field, radiated from coaxial-slot antenna is used to produce a temperature gradient in human tissue. Therefore the presented issue is a coupling of the electromagnetic field and the temperature field. For simplification a 2D model is considered. In order to conduct a full investigation of the temperature variation in the computational domain, Pennes equation, which takes into account blood perfusion rate, heat conduction effects of the tissue, heat generation due to metabolic processes and external heat sources, is solved. The microwave antenna is designed to operate at 2.45 GHz. Influence of the blood perfusion rate on temperature distribution in human tissue is investigated and at the end simulation results are presented.

1. INTRODUCTION

Interstitial microwave thermal therapy is an invasive type of hyperthermia treatment. Heat produced by microwaves (exceeding 40^{o}C) is used to kill pathological cells located deep with the human body. This special technique of cancer treatment seems to be the most effective one, because it delivers the heat directly at the site of the tumor and minimally affects surrounding the normal tissues. For interstitial hyperthermia high frequency needle electrodes, microwave antennas, ultrasound transducers, laser fibre optic conductors, or ferromagnetic rods, seeds or fluids are injected or implanted into the tumor [4, 5]. With these applicators high enough heat can be applied to induce thermonecrosis in tumors and cancerous tissues at the distance of 1 to 2 cm around the heat source. It is worth noting that this technique is suitable for tumors less than 5 cm in diameter [1]. Moreover, microwave hyperthermia is frequently used in conjunction with other cancer therapies, such as radiation therapy or chemotherapy [8]. It can increase tissue blood flow, thereby helping to oxygenate poorly oxygenated malignant cells. This method is now gaining new fields of applications, for instance in the treatment of liver, breast, kidney, bone and lung tumors [7]. There

* AGH, University of Science and Technology.

are many studies on the treatment of cancer using hyperthermia which demonstrate that this aspect is still important and more research is needed in this matter [3, 6] to make hyperthermia a simpler, safer, more effective and widely available treatment of cancer.

2. MATHEMATICAL AND GEOMETRICAL MODEL

The considered model of the coaxial-slot antenna (Fig. 1) consists of the central conductor, dielectric, outer conductor and a plastic catheter, which performs the protective function for all other elements of the antenna. The air gap with size d is located in the outer conductor. The antenna dimensions are taken from [10] and given in Tab. 1. In fact, the computational area is much larger than it is shown in Fig. 1, and the antenna width does not exceed 2 mm. Due to the axial symmetry of the model the cylindrical coordinates r, z, ϕ are used. The 2D model, which includes only half of the antenna structure and the surrounding human tissue, is sufficient for analysis. The 3D model of the antenna can be obtained by rotating the 2D model along the symmetry axis of the antenna (z axis for $r = 0$).

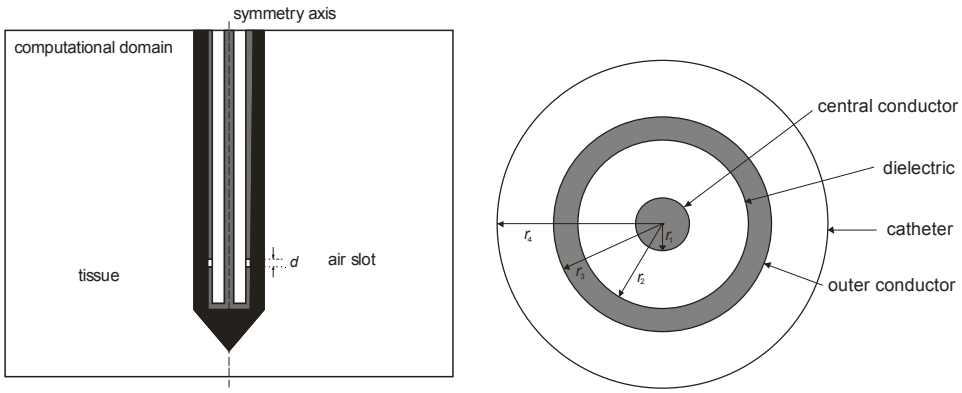

Fig. 1. Schematic view of the part of the coaxial antenna with the air slot (left) and cross section of the antenna with geometrical dimensions (right)

Table 1. Geometrical dimensions of the antenna in [mm]

radius of the central conductor	$r_1 = 0.145$
inner radius of the outer conductor	$r_2 = 0.470$
outer radius of the outer conductor	$r_3 = 0.595$
radius of the catheter	$r_4 = 0.895$
size of the air slot	$d = 1$

Derivation of the basic formulas let us start with the Maxwell's equations in the frequency domain defined as:

$$\nabla \times \boldsymbol{H} = \boldsymbol{J} + \mathrm{j}\omega \boldsymbol{D} \tag{1}$$

$$\nabla \times \boldsymbol{E} = -\mathrm{j}\omega \boldsymbol{B} \tag{2}$$

where $\boldsymbol{E}$ and $\boldsymbol{H}$ are the electric and magnetic field strengths respectively, ω is the angular frequency of the electromagnetic field and $\boldsymbol{J}$ is the vector of current density, which in conducting media is given by Ohm's law

$$\boldsymbol{J} = \sigma \boldsymbol{E} \tag{3}$$

where σ is the electrical conductivity of the medium. Moreover, $\boldsymbol{D}$ and $\boldsymbol{B}$ are respectively the vectors of electric displacement density and magnetic induction given in the form of material dependences:

$$\boldsymbol{D} = \varepsilon_0 \varepsilon_\mathrm{r} \boldsymbol{E} \quad , \quad \boldsymbol{B} = \mu_0 \mu_\mathrm{r} \boldsymbol{H} \tag{4}$$

where ε_r and μ_r are the relative permittivity and relative permeability of the medium, ε_0 and μ_0 are the permittivity and permeability of the vacuum, respectively. After taking into account the above dependences (3) to (4), the Maxwell's equations take the following form:

$$\nabla \times \boldsymbol{H} = \mathrm{j}\omega\varepsilon_0 \left(\varepsilon_r - \mathrm{j}\frac{\sigma}{\varepsilon_0 \omega} \right) \boldsymbol{E} \tag{5}$$

$$\nabla \times \boldsymbol{E} = -\mathrm{j}\omega\mu_0 \mu_\mathrm{r} \boldsymbol{H} \tag{6}$$

After applying the rotation operator to both sides of equation (5) and substituting equation (6) into the equation thus obtained, the following equation describing the magnetic field distribution in the studied area can be derived:

$$\nabla \times \left[\left(\varepsilon_\mathrm{r} - \mathrm{j}\frac{\sigma}{\varepsilon_0 \omega} \right)^{-1} \nabla \times \boldsymbol{H} \right] - \varepsilon_0 \mu_0 \mu_\mathrm{r} \omega^2 \boldsymbol{H} = 0 \tag{7}$$

Because in the time domain the vector of magnetic field strength is related with complex amplitude $\hat{\underline{\boldsymbol{H}}}$ by

$$\boldsymbol{H}(\boldsymbol{r}, t) = \mathrm{Re}\left[\hat{\underline{\boldsymbol{H}}}(\boldsymbol{r}) \mathrm{e}^{\mathrm{j}\omega t} \right] \tag{8}$$

thus equation (8) finally takes the form

$$\nabla \times \left[\underline{\varepsilon}_\mathrm{r}^{-1} \nabla \times \hat{\underline{\boldsymbol{H}}} \right] - \varepsilon_0 \mu_0 \mu_\mathrm{r} \omega^2 \hat{\underline{\boldsymbol{H}}} = 0 \tag{9}$$

where $\underline{\varepsilon}_\mathrm{r}$ is the complex relative permittivity of the medium defined by

$$\underline{\varepsilon}_\mathrm{r}(\omega) = \varepsilon_\mathrm{r} - \mathrm{j}\frac{\sigma}{\varepsilon_0 \omega} \tag{10}$$

Also the vector of electric field strength has a complex value which can be computed from the formula

$$\nabla \times \hat{\underline{\boldsymbol{E}}} = -\mathrm{j}\omega\mu_0 \mu_\mathrm{r} \hat{\underline{\boldsymbol{H}}} \tag{11}$$

The transverse magnetic (TM) waves are used in the presented model, so there are no electromagnetic field variations in the azimuthal direction. A magnetic field $\boldsymbol{H}$ has only the ϕ-component and an electric field $\boldsymbol{E}$ propagates in r-z plane. Therefore, it can be written as:

$$\hat{\underline{\boldsymbol{H}}}(\boldsymbol{r}) = H_\phi(r,z)\ \boldsymbol{e}_\phi \tag{12}$$

$$\hat{\underline{\boldsymbol{E}}}(\boldsymbol{r}) = E_r(r,z)\boldsymbol{e}_r + E_z(r,z)\boldsymbol{e}_z \tag{13}$$

Finally, in the axial-symmetry model, the wave equation takes the following scalar form

$$\nabla\times\left[\left(\varepsilon_\mathrm{r} - \mathrm{j}\frac{\sigma}{\varepsilon_0\omega}\right)^{-1}\nabla\times H_\phi\right] - \varepsilon_0\mu_0\mu_\mathrm{r}\omega^2 H_\phi = 0 \tag{14}$$

Complete definition of the model requires the determination of the appropriate boundary conditions for the electromagnetic field. For all metallic surfaces, the PEC (perfect electric conductor) boundary conditions are set as

$$\boldsymbol{n}\times\boldsymbol{E} = 0 \tag{15}$$

where $\boldsymbol{n}$ is the unit normal vector perpendicular to the surface. Moreover, the external boundaries of the computational domain, which do not represent a physical boundary (except the boundary at the z symmetry axis where $E_\phi(r) = 0$) have the so-called matched boundary conditions. They make the boundary totally non-reflecting and assume the form

$$\sqrt{\varepsilon - \mathrm{j}\frac{\sigma}{\omega}}\,\boldsymbol{n}\times\boldsymbol{E} - \sqrt{\mu}H_\phi = -2\sqrt{\mu}H_{\phi 0} \tag{16}$$

where $H_{\phi 0}$ is an input field incident on the antenna given by

$$H_{\phi 0} = \frac{1}{Z r}\sqrt{\frac{Z P_\mathrm{in}}{\pi\ln(r_2/r_1)}} \tag{17}$$

In above equation P_in is the total input power in dielectric, while r_1 and r_2 are the dielectric's inner and outer radii, respectively. Moreover, Z signifies the wave impedance of the dielectric which is defined as

$$Z = \sqrt{\frac{\mu_0}{\varepsilon_0\varepsilon_\mathrm{r}}} \tag{18}$$

The antenna's seed point, placed at the low-reflection external boundary of the coaxial dielectric cable, is modeled using a port boundary condition with the power level set to P_in.

In the simulation, the electromagnetic field is coupled with the temperature field. The phenomenon of heat transfer in biological tissues was described by Pennes [9], who in the mid-twentieth century derived so-called bioheat equation. In the case of steady-state analysis, it is expressed as follows

$$\nabla\left(-k\nabla T\right) = \rho_\mathrm{b}C_\mathrm{b}\omega_\mathrm{b}(T_\mathrm{b} - T) + Q_\mathrm{ext} + Q_\mathrm{met} \tag{19}$$

where T is the body temperature in K, k – the tissue thermal conductivity in W/(m^2 K), T_b – the blood vessel temperature in K, ρ_b – the blood density in kg/m^3, ω_b – the blood perfusion rate in 1/s, C_b – the blood specific heat in J/(kg K). Moreover, the described model takes into account both the metabolic heat generation rate Q_{met} in W/m^3, as well as the external heat sources Q_{ext} in W/m^3, which is responsible for the changing of the temperature inside the exposed body according to the following equation

$$Q_{ext} = \frac{1}{2}\sigma \, \hat{\underline{\boldsymbol{E}}} \cdot \hat{\underline{\boldsymbol{E}}}^{*} = \frac{1}{2}\sigma \left| \hat{\underline{\boldsymbol{E}}} \right|^2 \tag{20}$$

Since the computational area is only limited to part of the tissue, so it can be assumed that the heat exchange between parts of the same tissue does not occur and the boundary condition describing this process is as follows

$$\boldsymbol{n} \cdot \left(k \nabla T \right) = 0 \tag{21}$$

3. SIMULATION RESULTS

In the present example, the human tissue and the antenna are considered as homogeneous media with averaged material parameters The antenna operates at a frequency of f = 2.45 GHz. Electrical parameters of the tissue [2] and parts of the microwave antenna [10] are summarized in Table 2, and blood parameters used in the model are given in Table 3. Moreover, the tissue thermal conductivity is equal to k = 0.56 W/(m^2 K). and metabolic heat is specified as Q_{met} = 300 W/m^3.

Table 2. Electrical parameters used in the simulation

Elements of the model	ε_r	μ_r	σ **[S/m]**
human tissue	43.3	1	1.69
dielectric	2.02	1	0
catheter	2.60	1	0
air slot	1	1	1

Table 3. Physical parameters of blood taken to the bioheat equation

Tissue	ρ_b **[kg/m^3]**	C_b **[J/(kg K)]**	T_b **[K]**	ω_b **[1/s]**
blood	1020	3640	310.15	var

Equations (14) and (19) with appropriate boundary conditions were solved using the finite element method. The simulation results are summarized in Figures 2 – 4.

Fig. 2 shows the distribution of equipotential lines in the studied area for modulus of the magnetic field strength H and temperature T, respectively. They all have been calculated for the antenna input power level set to P_{in} = 2W. Moreover, for better visibility the scale of the first graph is cut off at H_{cut} = 10 A/m.

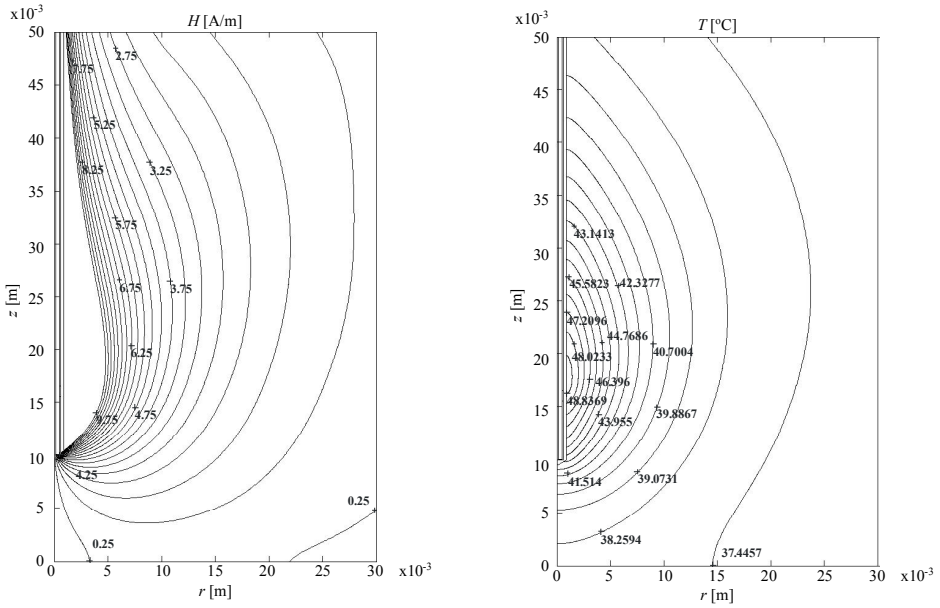

Fig. 2. Equipotential lines of the modulus of the magnetic field strength (left) and isothermal lines inside the computational domain (right)

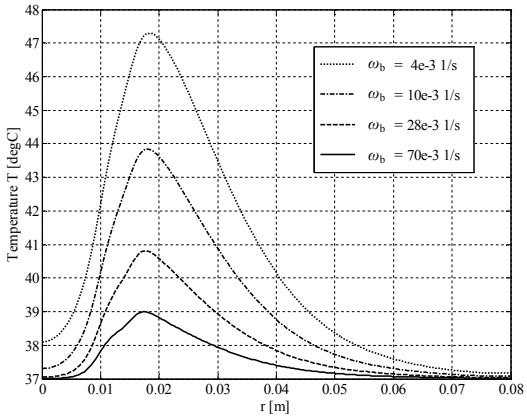

Fig. 3. Temperature distributions for different values of the blood perfusion rate along r = 0.0025 m

The remaining figures demonstrate the temperature distributions for different values of the blood perfusion rate ω_b, along two paths that pass through the human

tissue perpendicular to the antenna at the height of the air slot for $z = 0.016$ m (Fig. 3) and parallel to the symmetry axis of the antenna at a distance of 2.5 mm (Fig. 4). As expected, the tissue temperature decreases rapidly with the distance from the microwave applicator and its largest values occur near the antenna's air gap.

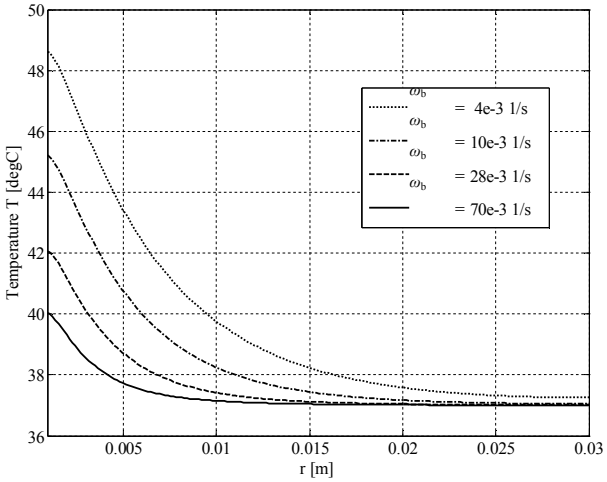

Fig. 4. Temperature distributions for different values of the blood perfusion rate along $z = 0.016$ m

4. CONCLUSIONS

The thermal analysis of the presented problem using the finite element method allows the estimation of the temperature distribution in the specified area. The adopted two-dimensional model represents a simplification of reality but it fully reflects the idea of treating pathological tissues using interstitial microwave hyperthermia and can be used to evaluate the actual temperature distribution in the three-dimensional case. The demonstrated plots show that the temperature decreases rapidly with the distance from the microwave applicator. Moreover, the therapeutic operating area where temperature exceeding 40°C depends on the tissue blood flow, which in turn has different values for tissues with different degree of vascularization and level of pathological changes. Generally, the increase in blood perfusion rate reduces the temperature induced inside the tissue under the same external conditions. This explains why tumors, characterized by lower blood flow, may become warmer during hyperthermia treatment than normal healthy tissues. On the other hand, hyperthermia in conjunction with radio- or chemotherapy can increase tissue blood flow, thereby helping to oxygenate poorly oxygenated malignant cells. This method is now gaining new fields of applications, e.g., in the treatment of liver, breast, kidney, bone and lung tumors.

REFERENCES

[1] Baronzio G.F., Hager E.D., *Hyperthermia in Cancer Treatment: A Primer*, Landes Bioscience and Springer Science + Business Media, New York, 2006.

[2] Gabriel C., Gabriel S., Corthout E., The Dielectric Properties of Biological Tissues: I. Literature Survey, *Physics in Medicine and Biology*, vol. 41, no.11, 1996 p. 2231-2249.

[3] Gas P., Temperature inside Tumor as Time Function in RF Hyperthermia, *Electrical Review*, vol. 86, no. 12, 2010, p. 42-45.

[4] Habash R.W.Y., Bansal R., Krewski D., Alhafid H.T., Thermal Therapy, Part 2: Hyperthermia Techniques, *Critical Reviews in Biomedical Engineering*, vol. 34, no. 6, 2006, p. 491-542.

[5] Hurter W., Reinbold F., Lorenz W.J., A Dipole Antenna for Interstitial Microwave Hyperthermia, *IEEE Transaction on Microwave Theory and Techniques*, vol. 39, no. 6, 1991, p. 1048-1054.

[6] Kurgan E., Gas P., Influence of Tissue Parameters on Deep Body RF Hyperthermia, *Poznan University of Technology Academic Journals. Electrical Engineering*, vol. 63, 2010, p. 63-68.

[7] Lin J.C., Wang Y.J., Interstitial Microwave Antennas for Thermal Therapy, *International Journal of Hyperthermia*, vol. 3, no. 1, 1987, p. 37-47.

[8] McPhee S.J., Papadakis M.A., Rabow M.W., *Current Medical Diagnosis and Treatment 2012*, McGraw-Hill, 2011.

[9] Pennes H.H., Analysis of Tissue and Arterial Blood Temperatures in the Resting Human Forearm, Journal of Applied Physiology, vol. 1, no. 2, 1948, p.93-122.

[10] Saito K., Taniguchi T., Yoshimura H., Ito K., Estimation of SAR Distribution of a Tip-Split Array Applicator for Microwave Coagulation Therapy Using the Finite Element Method, *IEICE Transaction on Electronics*, vol.E84-C, no.7, 2001, p. 948-954.